Critical Binder-to-Powders Coverage Ratio for Faster Graphite/SiOx Electrode Formulation Optimization

Clément Meyssonnier, Amina Merabet, Nicolas Dupré, Cyril Paireau, Bernard Lestriez

▶ **To cite this version:**

Clément Meyssonnier, Amina Merabet, Nicolas Dupré, Cyril Paireau, Bernard Lestriez. Critical Binder-to-Powders Coverage Ratio for Faster Graphite/SiOx Electrode Formulation Optimization. Small Methods, 2024, 8 (8), pp.2301370. 10.1002/smtd.202301370 . hal-04372607

HAL Id: hal-04372607
https://hal.science/hal-04372607v1

Submitted on 5 Jan 2024

HAL is a multi-disciplinary open access archive for the deposit and dissemination of scientific research documents, whether they are published or not. The documents may come from teaching and research institutions in France or abroad, or from public or private research centers.

L'archive ouverte pluridisciplinaire **HAL**, est destinée au dépôt et à la diffusion de documents scientifiques de niveau recherche, publiés ou non, émanant des établissements d'enseignement et de recherche français ou étrangers, des laboratoires publics ou privés.

Critical Binder-to-Powders Coverage Ratio for Faster Graphite/SiO_x Electrode Formulation Optimisation

Clément Meyssonnier[1,2], Amina Merabet[1], Nicolas Dupré[1], Cyril Paireau[2], Bernard Lestriez[1]

[1] Nantes Université, CNRS, Institut des Matériaux de Nantes Jean Rouxel, IMN, Nantes F-44000, France

[2] Armor Battery Films, 7 Rue de la Pelissière - 44118 La Chevrolière

bernard.lestriez@cnrs-imn.fr

Abstract

Mastering electrodes' formulations is a complex and tedious task, because for each composition of electroactive material(s) it is necessary to adjust the inactive additives nature and content to optimize battery performance. In this direction, we propose to adjust the amount of binder to the surface developed by all of the powders involved in the composition of the electrode, i.e. the electroactive materials and electronic conductive additives~~; this in order to guarantee or approach for different electrode compositions the same level of mechanical toughness~~. This concept, introduced here as binder-to-powders coverage ratio, relies upon the micromechanical models developed in the field of polymer-based composite materials. The validity of this new electrode formulation parameter is shown here for two different SiO_x/Graphite blends, which differ in the type of graphite, and for blends of two different binders, polyacrylic acid and styrene−butadiene rubber. At the optimal coverage ratio, a satisfactory capacity retention is obtained in full cell with an ethylene carbonate free and fluoroethylene carbonate rich electrolyte.

1. Introduction

In an effort to increase the energy density of lithium-ion batteries, silicon suboxide (SiO_x, x ~ 1) is being considered as a high capacity negative electrode material (1250-1750 mA h g^{-1}) because the volume change of SiO is less than that of pure Si and thus exhibits higher reversibility than the latter.[1,2,3] However, the volume change of SiO during lithiation/delithiation (1.6-2 times) is still significantly higher than that of graphite (1.1 times) and thus a careful binder optimization is required to stabilize the composite electrode structure upon an extended cycling.

The most suitable binders for SiO_x-based electrodes are generally the same as those for silicon-based electrodes, since these two types of electrodes must be resilient to repeated volume variations of the electroactive material. To be effective, it is generally observed that the binder must have adhesive functional groups towards the surface of the electroactive particles and have a high rigidity and therefore a high resistance to deformation in the presence of the liquid electrolyte, in order to maintain the contacts between the electroactive particles and thereby the cohesion of the electrode film.[4] [4] For silicon, the sodium salt of carboxymethyl cellulose (CMC), sodium alginate, and polyacrylic acid (PAA) are three widely used simple commercial binders.[5,6] [5,6] Their -COOH and/or COONa functions, depending on their neutralization ratio x, in $COOH_{1-x}Na_x$, make it possible to form strong and numerous hydrogen and/or covalent bonds with surfaces of the SiO_x or SiO_2 type, common to Si and to the SiO_x electroactive materials, as well as equally strong and numerous intra and interchain bonds which greatly limit their stretchability, and their affinity with the solvents of the electrolyte and consequently their plasticization by the latter. The better retention of the microstructure of the electrode film also enables minimization the continuous formation and growth of the SEI, because the latter is less destabilized by the slightest relative displacements and frictions of the electroactive particles.[7,8] [7,8] The COOH or COONa functions and the non- or low penetration of electrolyte solvents in these polymers also give them artificial SEI/passivation layer properties. Indeed, the layers formed by these binders on the surface of the electroactive particles constitute a non-permeable boundary between the latter and the electrolyte that therefore prevents electrons transfer and electrochemical reduction of the electrolyte.[5,9,10] [5,9,10] In addition, the transport of lithium through these binder layers would be possible thanks to the COOH or COONa functions, once transformed into COOLi, after the initial reduction step.[11].[11]

Many works have proposed optimizations of these binders, by playing on: (i) the neutralization ratio (and therefore the pH of the electrode slurry) and the molar mass, to play on the rheology of the slurry and the morphology of the electrodes; (ii) their chemical or physical cross-linking (by coordination with multivalent cations),[12,13], [12,13] to increase their rigidity; (iii) the modulation of their chemical structure by using copolymers or by mixing them with other polymers to, on the contrary, increase their flexibility.[14].[14] Finally, advanced macromolecular structures are also developed so as to present self-healing properties, and thus ideally form a glue capable of repairing, cycle after cycle, the mechanical damage that occurs in the electrode film.[15].[15]

Even if the most effective polymer binders make it possible to properly maintain the microstructure of the electrode film and thus ensure satisfactory cyclability in a laboratory half-cell against lithium metal, the lack of stability of the SEI generates a loss of lithium cycle after cycle still too large to consider the integration of electrodes solely based on Si or SiO_x in full lithium-ion commercial cells. Moreover, the

confinement imposed by the casing of commercial cells generates, in response to the very large volume variations of these electrodes, mechanical stresses so high that they cause damage to the other components of the cell (current collectors, separators), accelerating the end of life.[16,17,18]. The initial coulombic efficiency (ICE) of SiO_x electrodes is also very low due to the irreversible formation of lithium silicates, in addition to electrolyte degradation and solid electrolyte interphase (SEI) formation.[2,3].

For all these reasons, current research has focused on the integration of negative electrodes containing mixtures of Si or SiO_x and graphite. The dilution of the former in the latter makes it possible to significantly reduce the variations in volume of the electrodes as well as the destabilization of the SEI and the loss of lithium. The binders used in electrodes based on Si/Gr or SiO_x/Gr mixtures are identical to those of graphite electrodes, i.e. the mixture of CMC and SBR,[19], or identical to those evaluated for Si or SiO_x electrodes, or derivative formulations. For example, Komaba and co-workers reported the use of a partially neutralized poly(acrylic acid-co-hydroxymethyl acrylate) (PAA-co-HEMA) binder, chemically cross-linked by a diallyl ether cross-linker for a SiO@C/Acetylene Black(AB)/binder composition of 80:10:10.[8,20]. The electrochemical performance of the electrode was further improved by employing ''maturation'' treatment subsequently to the fabrication of the electrode film, and in which pre-dried electrode films on Cu foil are stored in 80 to 90% relative humidity for several days before the final drying step. Such ''maturation'' treatment greatly improves the mechanical strength of the electrode film.[21,22]. Jolley et al, reported the use of a poly(acrylic acid)-grafted styrene-butadiene rubber (PAA-g-SBR 1:5) with 80% partially neutralized Na-PAA as the 1:1 binder system for Si/Gr-based electrode. ~~The PAA-g-SBR graft copolymer was synthesized by grafting ter-butyl acrylate onto SBR.~~ The PAA-g-SBR/Na-PAA binder system was found to provide superior electrochemical performances to that of a Na-PAA/SBR system.[23].

In general, it is difficult to rationalize the work in the literature on the formulation of negative electrodes based on Si/Gr or SiO_x/Gr because many parameters vary from one study to another, such as: the Si/Gr or SiO_x/Gr ratio, the nature of the graphite which may even consist of a mixture of different graphites, the size and shape of the various electroactive particles, the nature and quantity of conductive additive, the formulation of the electrolyte, the loading and porosity of the electrodes, the solvent content in the slurries, the drying conditions. The multiplicity of these parameters also makes the formulation work tedious, because for each composition of electroactive material(s) it is necessary to adjust the formulation of its electrode to optimize battery performance. The search for simple relationships making it possible to adjust *a priori* the formulation of the electrodes, on the basis for example of the characteristics of the electroactive materials, is highly desirable. In this direction, we have in the past proposed to adjust the amount of binder to the surface developed by all of the

powders involved in the composition of the electrode, i.e. the electroactive material and electronic conductive additive; this in order to guarantee or approach the same level of mechanical properties for different electrode compositions.[24]. This concept, rationalized here as binder-to-powders coverage ratio, Γ, will be developed later. Its pertinence is for example observable in the study by Jeschull *et al.*[9]. Along the same lines, the study by Ambrock *et al.* suggest that the total surface developed by the electronic conductive additive could be adjusted to the surface developed by the electroactive material; this in order to tune similar electrical properties for different electrode compositions.[25]. Systematically adjusting the solvent content in the electrode slurry so as to give it equal rheological properties has been proposed by Xiong *et al.*; this in order to reach the same quality of distribution of the constituents in the electrode film for different electrode compositions.[26]. Finally, comparison of long-term electrochemical performance of Si/Gr or SiO_x/Gr electrodes needs to be always collected by using the same mass-loading with the constant electrolyte and additive.[1,27].

Theoretical background for the binder-to-powders coverage ratio

Standing on the micromechanical models developed in the field of polymer-based materials,[28,29], it can be assumed that the cohesion and the adhesion of composite electrodes are controlled by the strength of the binder bridges, σ_{int}, at the interfaces between neighboring particles and with the current collector[24,30] and ref therein

$$\sigma_{int} = a\Sigma f \quad (1)$$

where Σ is the areal density of polymer strands that are anchored on both sides of the interface. A polymer strand is a portion of a chain, each end of which is in contact with a point on the surface of a particle or of the collector and adhering to it. Thus, the same chain folded at an interface creates a multi-stranded bridge. The second parameter, f, is the strength of the anchoring bonds or the force to break a covalent bond in the polymer chain if the latter is weaker than the former. It depends on the strength of the interfacial interaction (van der waals, hydrogen) or bond (ionic, covalent) between the polymer moieties (lateral functional groups or monomeric unit of the chain skeleton) and the chemical groups or atoms present at the contact point with the electroactive and conductive additive particles, and the current collector. The parameter *a* reflects the intrinsic toughness of the polymer, depending on its molecular structure (see below).

In the case of Si and SiO_x materials, the electrochemical (de)lithiation reaction involves volume variations of the electroactive particles, and consequently mechanical stresses on the binder bridges between the particles and with the current collector in the electrodes. If the rupture of the binder bridges is synonymous with loss of electrical contact and therefore of electroactivity of the particles concerned, then it is expected that the cyclability of the electrodes depends on the mechanical

strength of the binder bridges. This hypothesis is supported by experimental relationships observed between cyclability of Si-based electrodes and the expected toughness of polymer binder bridges, based on the binder amount, localization in the electrode, molecular architecture and intrinsic mechanical properties.[6,13,21,22] Visualization of polymer bridges and the direct measurement of their toughness is experimentally very difficult due to their nanometric size and because they are buried at interfaces. Müller *et al.* employed X-ray nano-tomography and backscattered scanning electron microscopy with sufficient resolution and contrast to segment the carbon black-binder domain and quantified their delamination from the active material surface as a function of cycle number in real electrode.[30] Maver *et al.* used the atomic force microscopy (AFM) to probe the interaction between silicon and CMC, depending on pH condition preparation on a model system (silicon wafer).[31] Their measurements show a force an order of magnitude bigger as well as longer interaction distances for a CMC/citric acid binder compared to CMC. Other work by Tranchot et al. showed superior mechanical properties and cyclability of Si-based electrodes prepared with the CMC/citric acid binder compared to CMC.[32]

Parameters or factors that can typically contribute to the increase in σ_{int} and therefore in cyclability improvement are: increase in amount of binder at constant particle size (⇔ increase in Σ);[6,33] increase in particle size at constant binder level (⇔ increase in Σ);[9,34] increase in the length of the polymeric chains of the binder (because longer chains can fold more times thus multiplying Σ and f);[35] increase of the strength of the interactions or bonds between the binder and the surface of the particles or the current collector (increase in f);[36] increase of the intrinsic toughness of the polymer, for example through cross-linking or enhanced crystallization (increase in *a*).[13,37]

All these considerations show that this problem is complex and system dependent. However, it is crucial for optimizing the mechanical and electrochemical properties of the electrodes. Rationalization is therefore eminently necessary, which the approach developed here allows. For a given polymer binder, the parameter f can be documented through spectroscopic characterizations probing the nature and thus revealing the strength of the anchoring bonds.[4,37,38] The experimental determination of Σ in a real composite electrode is hardly possible. However, and in a first approximation, it can be rationalized as the ratio of the binder mass to the sum of the geometrical surface area of the electroactive and conductive particles, assuming that the binder homogeneously and equally distributes at the surface of all particles.

$$\Sigma \propto \frac{binder\ mass\ (g)}{powders\ surface\ area\ (m^2)} = \Gamma \qquad (2)$$

where Γ (mg m^{-2}) is the binder-to-powders coverage ratio. Γ(m) also corresponds to the theoretical thickness of the binder layer covering the particles in the electrode, which can be realized converting the binder mass into a volume (through its density). The assumption behind eq. 2 is crude because the binder does not adsorb to the surface of the electroactive particles (AM) in the same way as the particles of conductive additive (C), because the strength of the binder/AM and binder/C interactions is different,[38],[38] and because binder segregation phenomena can be observed during the mixing and drying of the electrode inks. Indeed, a fraction of the binder can migrate to the surface of the electrode,[39],[39] and another can be concentrated in the smallest pores and in particular at the location of the contacts between particles.[40].[40] In addition, insufficient mixing of the ink can result in a heterogeneous distribution of the binder in the bulk of the electrode.[41].[41] Nevertheless, if it is possible to minimize the segregation phenomena, which depend on the manufacturing conditions of the electrodes, the use of the parameter Γ appears to be a convenient way to compare the effectiveness of a binder in different formulations of electrode and compare different binders with each other. Finally, the identification of a critical value of Γ for which the optimization of the mechanical properties of an electrode would be carried out would facilitate the extrapolation of new electrodes formulations.

Here, the relevance of Γ is shown for SiO_x/Gr electrodes prepared with two different graphites, GHDR 15-4 and SFG6L, in different proportions, 60:40 and 90:10, and made with different content of a binder blend, PAA and SBR, also varied in different proportions. The physical properties of these electrodes and their cycling behaviour, in half cells and in full cells for selected formulations, was studied as a function of Γ.

Table 1: Weight percentage composition of the electrodes and their critical ratio.

	Name	Coverage ratio Γ * (mg m^{-2})	SiO_x/Graphite balance	SFG6L/GHDR balance	Binder (wt%)			Active materials (wt%)			C45 (wt%)
					PAA	SBR	LiOH	SiO_x	SFG6L	GHDR	
10SFG-x*PAA*	10SFG-2PAA-2SBR	8.3	23:77	10:90	2.2	2.5	< 0.0	21.0	7.1	63.6	3.6
	10SFG-5PAA-2SBR	14.6			5.5	2.5	0.6	20.1	6.8	60.9	
	10SFG-7PAA-2SBR	17.2			6.9	2.5	0.1	19.9	6.7	60.4	
	10SFG-8PAA-2SBR	20.4			8.3	2.7	0.1	19.5	6.6	59.2	
	10SFG-11PAA-2SBR	24.9			10.6	2.5	0.1	19.0	6.4	57.7	
40SFG-x*PAA*	40SFG-4PAA-2SBR	8.3	23:77	40:60	4.0	2.5	< 0.0	20.9	28.1	42.1	2.4
	40SFG-6PAA-2SBR	11.2			6.0	2.5	0.1	20.4	27.5	41.1	
	40SFG-8PAA-2SBR	14.9			8.0	2.9	0.1	20.4	24.9	41.3	
	40SFG-10PAA-2SBR	16.3			9.6	2.5	0.1	19.5	26.4	39.5	

	40SFG-12PAA-2SBR	20.1			12.0	2.5	0.2	19.0	25.6	38.4	
	40SFG-15PAA-2SBR	24.9			14.9	2.5	0.2	18.3	24.6	37.0	
40SFG-x*SBR*	40SFG-4PAA-2SBR	8.3	23:77	40:60	4.0	2.5	< 0.0	20.9	28.1	42.1	2.4
	40SFG-4PAA-4SBR	11.0			4.0	4.5	< 0.0	20.4	27.5	41.2	
	40SFG-4PAA-6SBR	13.9			3.9	6.5	< 0.0	19.9	26.9	40.3	
	40SFG-4PAA-10SBR	20.2			4.0	10.5	< 0.0	19.0	25.6	38.5	

* In equation 2, the "Binder mass" is the whole binder mass in the electrode (PAA + SBR) and the "Powder surface area" corresponds to the entire surface area of the electrode powders (SiO_x + GHDR 15-4 + SFG6L + C45) estimated from their BET surface area and their respective mass in the electrode.

Results and discussion

Electrochemical measurements – Half cells

Cycling behaviour has thus been investigated for various coverage ratios for two graphite active materials GHDR 15-4/SFG6L balances, 90:10 and 60:40, with varying PAA amounts while keeping the SBR one constant (see 40SFG-x*PAA* & 10SFG-x*PAA* series in Table 1). Figure 1a & b display specific capacities versus cycle number for 40SFG-x*PAA* & 10SFG-x*PAA* electrodes. Every electrode composition provides 777 ± 7 mA h g^{-1}_{AM} specific capacity for the first lithiation and 622 ± 3 mA h g^{-1}_{AM} during the second one. The latter corresponds to a reversible specific capacity for SiO@C ≈ 1645 mA h g^{-1}_{SiOx}, taking into account the 20:80 SiO@C/Gr mass ratio in the composition of the electrode and a specific capacity of 370 mA h g^{-1}_{Gr} for graphite. The irreversible capacity at the first cycle is ≈ 150 mA h g^{-1}_{AM}. Again, taking into account the composition of the electrode and a typical irreversible capacity of 30-40 mA h g^{-1}_{Gr} for the graphites[42] [42], it gives an irreversible capacity of ≈ 540-595 mA h g^{-1}_{SiOx} for our SiO_x, which is consistent with previous reports and is attributable to the irreversible lithiation reaction of the silica from the SiO_x component in addition to the SEI formation[43,44,45,46] [43,44,45,46]. This very low ICE is identified as a barrier to the practical use of SiO_x in full cells in which the lithium source is limited.

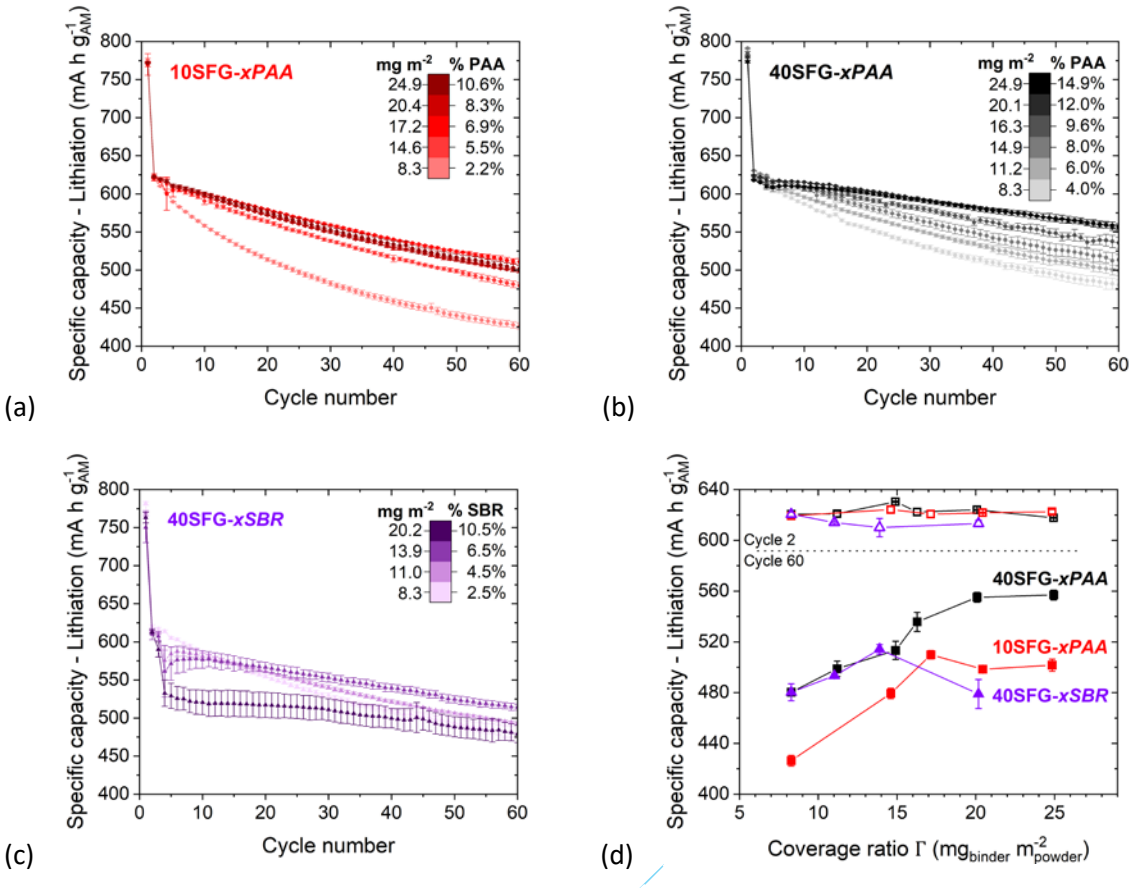

Figure1. Cyclability of a SiO_x/Graphite electrode with GHDR 15-4/SFG6L ratio of 90:10 or 60:40 for different binder amounts: (a) 10SFG-xPAA, (b) 40SFG-xPAA, (c) 40SFG-xSBR. (d) Lithiation specific capacity vs. binder-to-powders coverage ratio for the three electrode series at cycle 2 and 60.

Although all electrodes, whatever their composition, deliver the same nominal specific capacity at the early stage of cycling, they then gradually diverge from each other. For the 40SFG-*xPAA* series, the higher the binder amount is, the higher the specific capacity after 60 cycles is, while for the 10SFG-*xPAA* series the specific capacity increases and then levels at binder amount of 6.9%. These observations are made for both GHDR 15-4/SFG6L balances. To better assess the effect of particles coverage, specific lithiation capacities are plotted as a function of the coverage ratio for cycles 2 and 60 for the two investigated GHDR 15-4/SFG6L balances Figure 1d. The coverage ratio naturally increases as the PAA amount increases (Table 1). The retained capacity after 60 cycles clearly increases with the coverage ratio. For the 10SFG-x*PAA* electrodes, we note a specific capacity increase of 19.6% from 8 mg m^{-2} (2.2% PAA) to 17 mg m^{-2} (6.9% PAA). The trend is overall similar for 40SFG-*xPAA* electrodes. The specific capacity increases by 15.6% from 8 mg m^{-2} (4% PAA) to 20 mg m^{-2} (12% PAA) after 60 cycles. Interestingly, in both cases, the specific capacity plateaus for coverage ratio above 17-20 mg cm^{-2}, although the proportions of binder are very different between GHDR 15-4/SFG6L balances. It suggests this coverage ratio value is optimal with respect to specific capacity retention, as the further addition

of binder does not lead to a performance increase. However, it could be possible that a binder excess may penalize the alloying reaction by hindering charges (electrons and lithium ions) transfer due to an excessive particles coverage[33]. To check this hypothesis, we estimated the average polarization (See Equation S1)[47] for each cycle at C/5 rate i.e. from cycle 4 to 60 (Figure S1). We observed that this average polarization does not vary much with the coverage ratio (Figure S1a-b), indicating minimal charge transfer limitations at high PAA content.

The influence of the coverage ratio was then studied for various SBR amounts while keeping the PAA one constant (see 40SFG-x*SBR* series in Table 1). Indeed, many batteries in the industry are cylindrical cells in which the electrodes are rolled around a mandrel. This type of assembly requires flexible electrodes in order to prevent their cracking and delamination from the current collector due to the curvature imposed by this type of cell configuration. SBR is a binder that improves the flexibility of the electrode and its adhesion to the current collector. Unfortunately, it does not provide the necessary viscosity properties for the coating of electrode slurry on the current collector. This is why it is used in complement to PAA or CMC, where PAA or CMC provides part of the mechanical properties of the electrode as well as the viscosity necessary for good rheology of the slurry during coating. Figure 1c shows the lithiation capacity as a function of the cycle number for these electrodes. For the first three cycles at C/20-rate the analysis is the same than previously for 10SFG-x*PAA* and 40SFG-x*PAA* studies. A first lithiation capacity of 766 ± 13 mA h g^{-1}_{AM} and a second 615 ± 4 mA h g^{-1}_{AM} with initial coulombic efficiency of 77 ± 1%.

Then, a marked capacity drop appears from cycle 4 onwards when the cycling rate is increased from C/20 to C/5. The capacity drop is proportional to the SBR content in the electrode, e.g. -0.5%, -6.7%, -9.0% and -13.7% between cycles 3 and 4 for 2.5%, 4.5%, 6.5% and 10.5% SBR-based electrodes, respectively. This loss of capacity is directly correlated to the increase in polarization with the SBR amount as shown in Figure S1c. This increase in polarization implies that the cell voltage reaches the 10 mV cut-off voltage earlier and then starts the constant voltage step (CV) at the end of lithiation. Since the two hours' limitation of the CV step is reached before the full lithiation of the electrodes, a decrease in capacity proportionally to the polarization is observed.

During the next few cycles, the polarization decreases allowing the total capacity of the active materials to be fully utilised for all the electrodes except the 10.5% SBR one. The polarization of the latter is so severe that the electrode never reaches a fully lithiated state leading to a low but stable capacity, likely due to a lower mechanical stress in the electrode. After 60 cycles ageing, the performance reach 480 ± 6 mA h g^{-1}_{AM}, 493 ± 2 mA h g^{-1}_{AM}, 514 ± 4 mA h g^{-1}_{AM} and 479 ± 11 mA h g^{-1}_{AM} for 2.5%, 4.5%, 6.5% and 10.5% SBR-based electrodes, respectively. An increase in performance is seen with increasing SBR amount in the electrode with the exception of the electrode with 10.5% SBR.

When these capacities are plotted as a function of the coverage ratio (Figure 1d), it appears that the 40SFG-x*SBR* electrodes show similar capacity retention than the 40SFG-x*PAA* ones up to the coverage ratio of 14 mg cm^{-2}. This result suggests that SBR and PAA are equivalent binders to maintain electrode functioning during cycling. However, when we plot the mean value of polarization from cycle 4 to 60 (Figure S1d), we note a polarization increase of 0.6 mV per coverage ratio unit due to PAA increase against 4.8 mV per coverage ratio unit due to SBR increase. The addition of SBR seems to improve the mechanical structure of the electrode in the same manner as PAA, but also leads to a significant increase in electrode polarization, making it less attractive than PAA in terms of binder and electrode component.

Finally, since the binder is an inactive constituent, it is important to check that if the increase in its concentration in the formulation improves the cyclability of the electrode, this is not at the expense of the gravimetric capacity of the latter. This is explored in Figure S2. As a conclusion, after 60 cycles the best performance are achieved for the optimal coverage ratio of 18-20 mg m^{-2}.

Mechanical and electrical characterizations

To shed some light on the electrochemical behaviour of these electrodes, characterizations of their mechanical and electrical properties were undertaken. For all series, an increase in peel strength is observed with increasing polymer content (coverage ratio) (Figure 2a). All compositions with coverage ratio of 8 mg m^{-2} show an adhesive force of 43 ± 8 N m^{-1}. For the coverage ratio of ~ 14-15 mg m^{-2}, the two formulations rich in PAA (10SFG-x*PAA* and 40SFG-x*PAA*) show the same peel strength, ≈ 65 N m^{-1}, while that rich in SBR (40SFG-x*SBR*) is much higher, with ≈ 140 N m^{-1}. For the coverage ratio of ≈ 20 mg m^{-2}, a distinction is made between the two formulations rich in PAA, the one containing the highest amount of SFG6L (40SFG-x*PAA*) showing a resistance of 64 ± 3 N m^{-1}, the one containing the lowest amount of SFG6L (10SFG-x*PAA*) showing a resistance of 120 ± 12 N m^{-1}, while the formulation rich in SBR (40SFG-x*SBR*) is even more superior, with 182 ± 4 N m^{-1}. SBR provides thus a clear strengthening of the electrode in terms of mechanical properties in comparison with PAA. In all cases, observation of the specimens after peeling shows that the rupture is of the cohesive type (Figure S3), and measurements, only carried out for the 40SFG-x*PAA* series, show that the quantity of electrode material which remains attached to the current collector decreases with the increase in peel force, confirming that the latter is a measure of electrode cohesion (Figure S3).

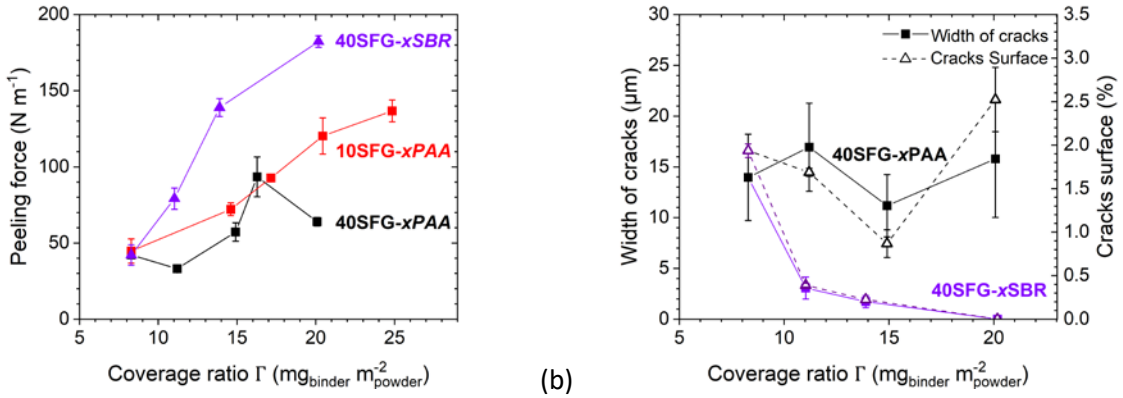

Figure2. (a) Peel force vs. binder-to-powders coverage ratio for the three electrode series. (b) Width and % of cracks observed at the electrode films surface after the winding test 40SFG-xPAA and 40SFG-xSBR.

To evaluate the influence of the binder composition on electrode flexibility, we carried out winding tests on electrode pieces rolled around mandrels of 3 mm diameter for 40SFG-x*PAA* and 40SFG-x*SBR* series (Figure S4a-b). Please note that in the first one the SBR content is kept constant at 2.5 wt% and the PAA content varies from 4 to 12 wt%, while in the second it is the reverse, the PAA content is kept constant at 4 wt% and the SBR one varies from 2.5 to 10.5 wt%. An images processing of the SEM pictures allowed to measure the crack widths (local thickness method[48] [48]) and the crack density (Figure S4c), which are plotted according to the coverage ratio Figure 2b. Whatever the amount of PAA, i.e. at constant SBR content (40SFG-x*PAA* series), cracks density and widths are similar, between 0.9 and 2.5% and between 11.2 and 15.8 µm, respectively. On the opposite, increasing the amount of SBR (40SFG-x*SBR* series) drastically decreases cracks density from 2.3% to 0.4% for 8.3 and 11.0 mg cm^{-2} and reach no measurable crack for 20.2 mg cm^{-2}. At the same time the crack width decreases from 14 ± 4 µm to 3 ± 1 µm and 0 (no crack). These observations confirm the benefit of the SBR binder for cylindrical battery type.

The comparison of Figures 1d, 2a, and 2b permits to affirm a relationship between the mechanical cohesion of the electrodes, which strengthens with the increase in the coverage ratio, and the electrochemical cyclability. This relationship is however not a direct one because, for example up to a coverage ratio of about 16 mg m^{-2}, the cohesion of the electrodes of the 40SFG-*xSBR* series is much higher than that of the 40SFG-*xPAA* series, but their cyclability are equal. This can be explained by the fact that the mechanical deformation, imposed on the electrodes during the peeling and winding tests, is higher than that imposed by the volume variations induced by the (de)insertion reactions of lithium in electroactive particles. Thus, although SBR is much more extensible than PAA, this property is apparently not required under cycling conditions. On the other hand, it appears essential to ensure

the mechanical integrity of the electrodes during battery assembly operations. At high coverage ratio, the 40SFG-*xSBR* series shows a drop in performance due to very high polarization of the electrodes (Figure S1).

To elucidate the origin of the latter, the electrical resistivity of the electrodes was measured. Before coming to this, it can be noted that the cyclability of the electrodes of the 10SFG-*xPAA* series is inferior to that of the 40SFG-*xPAA* series, although their mechanical properties are equivalent. Figure 3 clearly indicates a low resistivity around $2.0 \pm 0.4 \times 10^{-5}$ Ohm cm whatever the coverage ratio for the 40SFG-*xSBR* series. On the other hand, the 40SFG-*xPAA* one displays an increase from 2.4×10^{-5} to 1.4×10^{-2} Ohm cm for 8.3 and 14.9 mg m^{-2} respectively, and a plateau around 10^{-2} Ohm cm for higher coverage ratio. This result indicates that the higher polarization induced by the SBR binder does not come from an increase in the electrical resistivity but rather from ionic conductivity limitations, as proposed in other works[49,50] [49,50]. Interestingly, a smaller increase of the resistivity is noticeable for 10SFG-*xPAA* series from $\approx 10^{-5}$ to $\approx 10^{-4}$ Ohm cm by increasing the coverage ratio, compared to 40SFG-*xPAA*. Here, the electrons transfer in the electrode is surely affected by the different graphite balances between GHDR 15-4 and SFG6L. The increase in the quantity of SFG6L leads to an increase in the number of interparticle contacts, which constitute barriers to the transfer of electrons, all the more so as the binder is concentrated there[52,53] [51,52]. However, as shown by the superior cyclability of this 40SFG-*xPAA* series compared to the 10SFG-*xPAA* one, more numerous interparticle contacts favours the cyclability of the SiO_x/Gr electrodes.

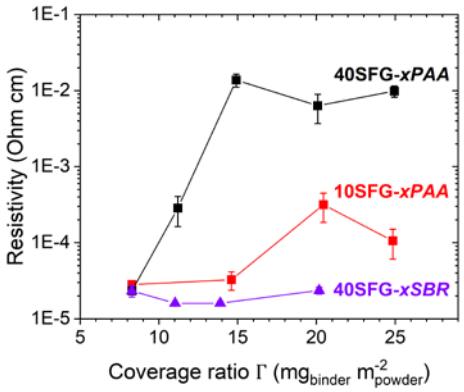

Figure 3. Electrical resistivity vs. binder-to-powders coverage ratio for the three electrode series.

Complementary understanding of the source of capacity loss during cycling was addressed by two methods. First, by studying whether the capacity loss is global or preferentially distributed over one of the two active materials, through a quantitative analysis of incremental capacity curves, and then by performing SEM-EDX characterizations of cycled electrodes cross sections.

Analysis of incremental capacity curves

The incremental capacity curves allow to clearly pinpoint and identify the potentials of the various electrochemical processes occurring within the SiO_x/Graphite electrodes[53] [53]. Each active material has its own signature depending on its reaction mechanism (See Figure S5). During delithiation, a marked transition appears between the part of the curve reflecting the electrochemical activity of graphite (below 270 – 290 mV at C/5) and that reflecting the activity of SiO_x (above 270 – 290 mV), suggesting a clear two-step delithiation, first graphite then SiO_x. We then considered that the capacity between 10 and 280 mV is attributable to graphite, while the capacity between 280 mV and 1 V is attributable to SiO_x only. This attribution is approximate in the graphite area, which contain a part of SiO_x contribution, but is correct in the SiO_x one. The comparison of SiO_x/Graphite incremental capacities at cycle 2 and 62 (Figure S5b), shows only a weak capacity loss within the graphite region whereas a significant capacity loss is observed in the SiO_x region. To prove this observation, we have written a code using Python to identify automatically the potential limit around 270 – 290 mV at C/5 which is sensitive to the current value and electrode resistivity evolution. We then integrated incremental capacity curves to calculate the capacity in both regions and results are shown in Figure 4a for 10SFG-x*PAA* and Figure 4b for 40SFG-x*PAA* series. In both cases, the capacity fading is clearly different between the graphite region and the SiO_x one. It appears that the capacity loss in the graphite region is moderate or even negligible, while the capacity loss mainly occurs in the SiO_x potential region and thus reflects the overall capacity fading observed for the whole electrode. The percentage of overall capacity loss attributed to graphite or to SiO_x at the 60th cycle is plotted as a function of the coverage ratio in Figure 4c. It shows that every formulation displays a low and similar capacity loss of ≈ 14-2% after 60 cycles in the graphite potential region. On the opposite, capacity losses occurring within the SiO_x potential region are between 49-31% for 10SFG-x*PAA* and 34-10% for 40SFG-x*PAA*. In addition, we certainly over-evaluate the capacity of graphite because ≈ 21% of the SiO_x capacity come from this potential range of 10-260 $mV_{vs\ Li+/Li}$. Therefore, the small loss of capacity in graphite area could be totally or partly due to the loss of SiO_x capacity, meaning that the capacity loss of graphite is surely lower than the 14-2% measured after 60 cycles. This result is not consistent with a scenario in which entire parts of the electrode are disconnected. In that case, the graphite contribution would decrease in the same proportion as that of SiO_x, which is not what is observed here. On the contrary, this result clearly indicates that the capacity fading mainly comes from the SiO_x particles disconnection from the percolating network.

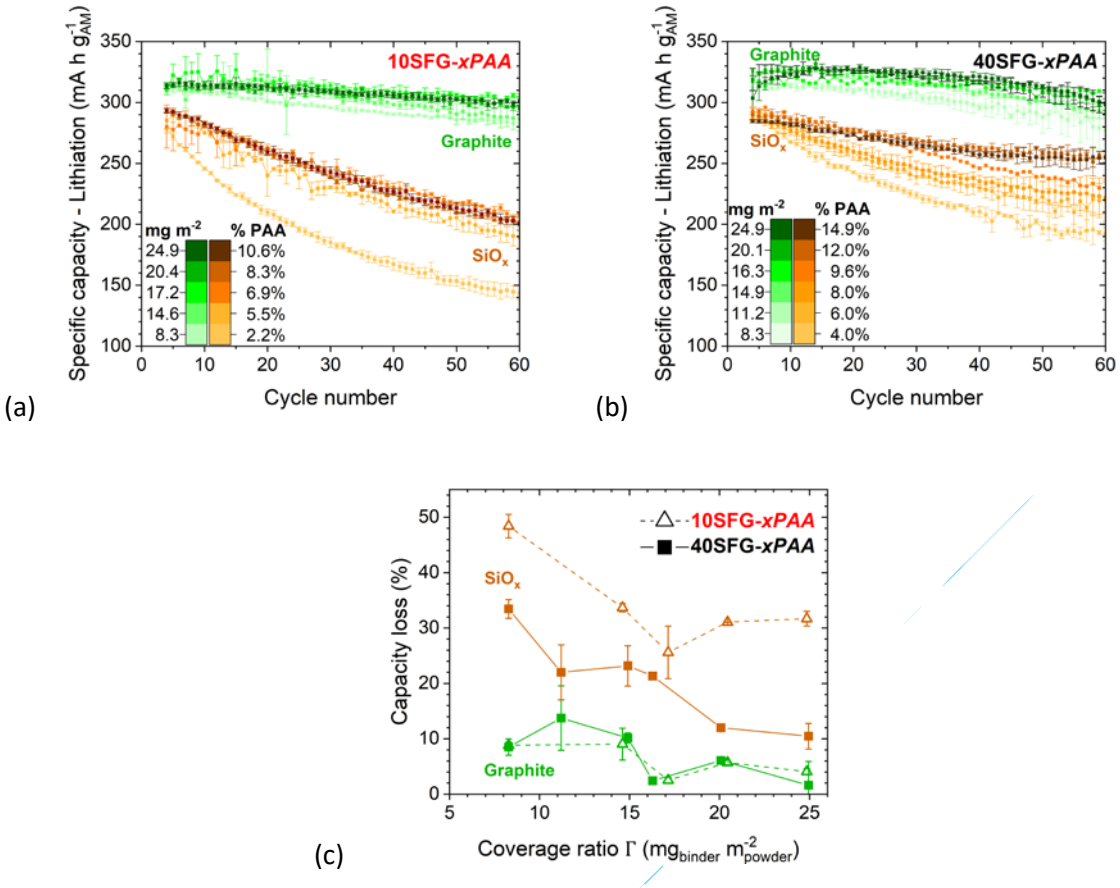

Figure 4. Delithiation specific capacity in the graphite and SiO_x potential windows for (a) 10SFG-xPAA and (b) 40SFG-xPAA series vs. cycle number. (c) Percentage of capacity loss in the graphite and SiO_x potential windows at the 60th cycle vs. coverage ratio for both series.

SEM-EDX characterizations

The 10SFG-11PAA-2SBR pristine electrode is observed in backscattered electrons mode at different magnifications (Figure 5a and b (× 3,000) and c (× 10,000)). The same images but in secondary electrons mode are given in Figure S6. One can very clearly distinguish: (i) in white the SiO_x particles, dense and angular, and the copper current collector, (ii) in grey with a spherical tendency the GHDR particles, displaying a lamellar and porous internal structure, and the SFG6L platelets. C45 carbon black also appears in grey in the form of agglomerates of variable dimensions, some of which can go up to almost 10 µm. Porosity filled with resin appears darker grey than the graphitic species and the conducting additive. The binder is indistinguishable. It can be noted that the internal porosity of the GHDR particles is for the most part filled with resin, which means that it is open, and therefore in battery probably wetted by the electrolyte. A fraction of this porosity, in black, generally in the center of the particles, has not been impregnated by the resin. It can also be seen that the distribution of the SiO_x particles is not homogeneous and that they are often gathered in bundles. The observation of non-calendered electrode cross-sections (not shown) suggests that there is very little fragmentation

of the SiO_x particles during the calendering step. SiO_x/Graphite contacts appear numerous, in some cases via C45 aggregates.

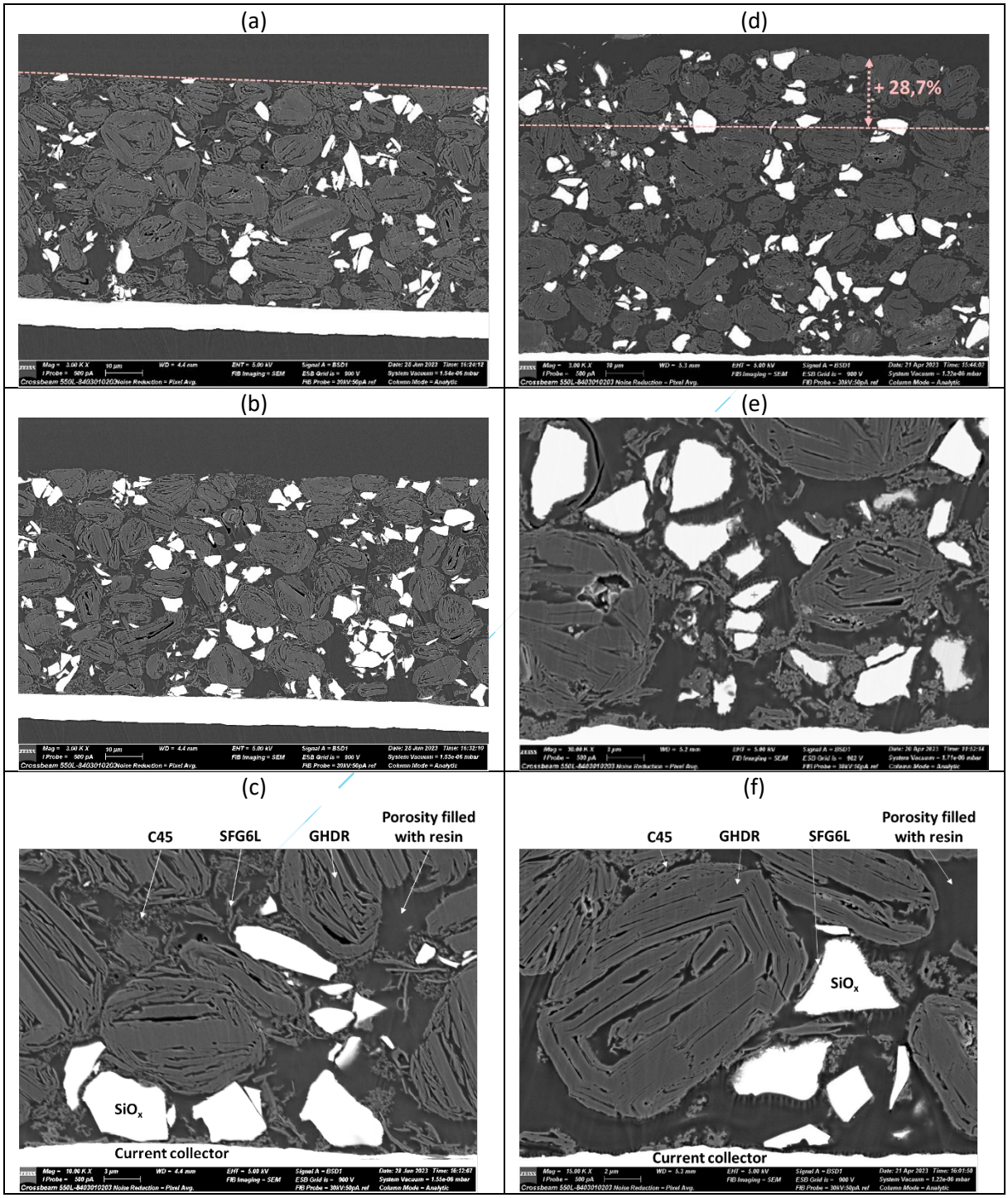

Figure 5. Cross section SEM observations (backscattered electrons) of (a-c) pristine and (d-f) cycled 10SFG-11PAA-2SBR electrode.

A 10SFG-11PAA-2SBR electrode was observed after 60 cycles. The general view (Figure 5d (× 3,000)) shows clearly the increase in thickness of the electrode film. On the same zone imaged in secondary electron mode (Figure S6d), the resin which impregnates the porosity of this electrode has in places a different appearance from that on the pristine electrode, in particular in the vicinity of the clusters of SiO_x particles, which may indicate that products present in the SEI may have dissolved in the resin before it polymerized or reacted with the resin. The SiO_x particles are still dense and do not appear to have been fractured by cycling. On the other hand, views at higher magnifications (Figure 5e (× 10,000), f (× 15,000), and Figure S7 (× 150,000)) show a modification of their surface which has become rough with the presence of a granular phase on this surface. These views also suggest that SiO_x/Graphite and SiO_x/C65 interparticle contacts are less frequent than in the electrode before cycling.

Chemical maps (elements C, O, F, P) were carried out by EDX, but this time on electrode sections carried out with FIB-SEM, without exposure to air of the sample between cutting and analyses. A view of the cross-section is presented in Figure S8a with the maps for the elements C, Si, and O in Figure S8b. Contrary to previous observations, the porosity of the sample is not filled with resin. This is the reason why the porosity seems lower than on the previous observations because the morphology is observed in the depth of the cut. The maps make it easy to identify GHDR (intense red) and SiO_x (intense purple and green) particles. The presence of C45 agglomerates and possibly PAA is detectable (pale red and green). In particular, disperse areas in green (O) with no counterparts in purple (Si) may correspond to binder agglomerates and/or electrolyte degradation species.

Analyzes with different electron beam acceleration voltages (4 and 10 kV) were performed. The higher the acceleration voltage, the deeper the sample is probed. Selected observations are shown in Figure S9. The comparison of the silicon and oxygen maps points clearly towards the presence of an oxygen-rich layer on the surface of the SiO_x particles (Figure S9c-f). The comparison of the carbon and oxygen maps makes it possible to identify the presence of a thinner layer, containing oxygen, on the surface of the graphite particles (Figure S9b-d). The Fluorine is present in the form of discrete deposits in a few places (Figure S9e). This is in agreement with previous observations by our group, in which species coming from the degradation of the electrolyte, such as LiF, appear as discrete patches on the surface of the silicon oxide particles[54] [54]. In the fluorine-rich spots, notably in the internal porosity of the GHDR particles, phosphorus (not shown), is also detected, indicating the presence of the usual degradation products containing those elements, such as LiF and $LiP_xO_yF_z$[54,55] [54,55]. The additional presence of residues of the $LiPF_6$ salt not eliminated by rinsing the electrode with DMC cannot be ruled out, especially within the porosities which are more difficult to rinse properly.

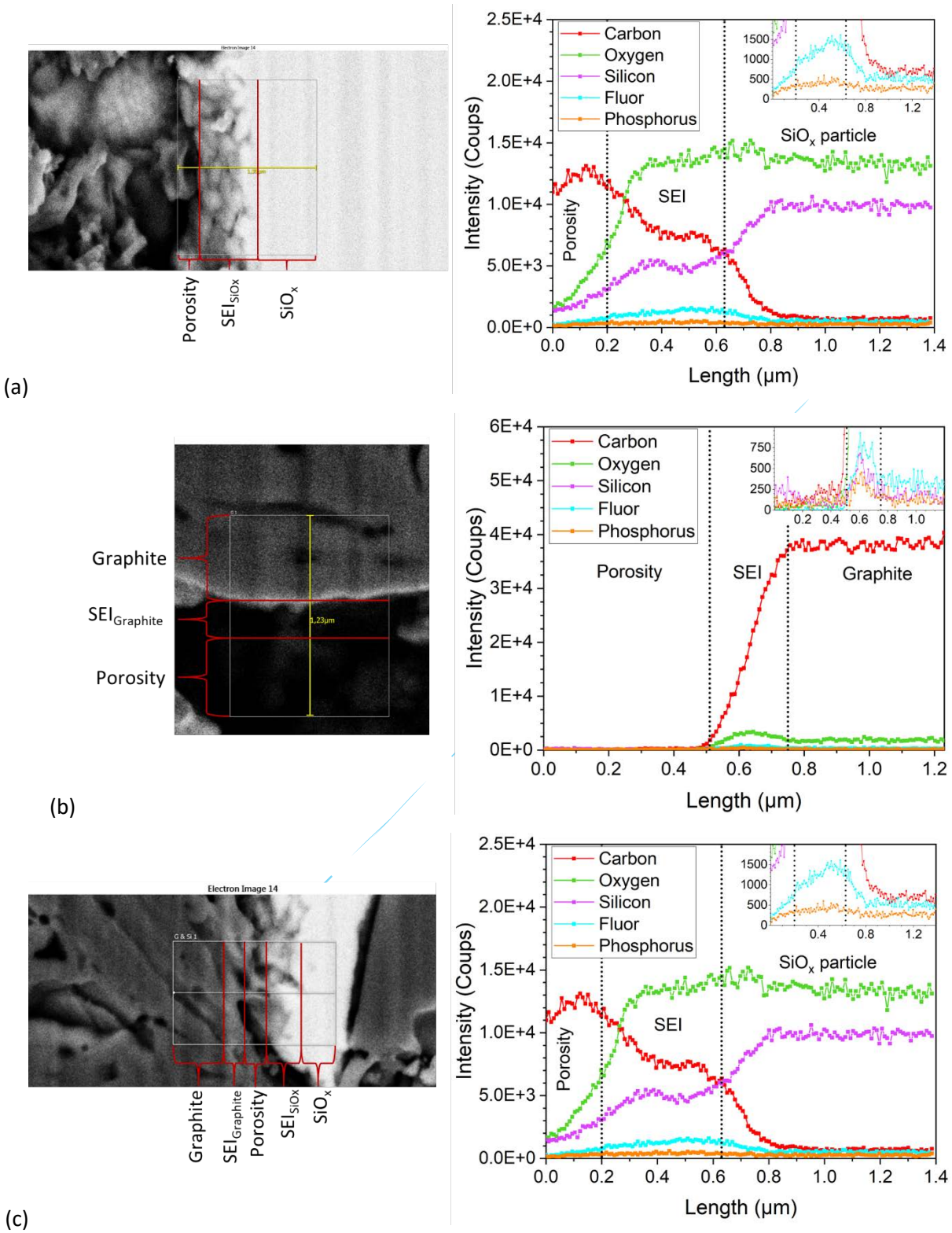

Figure 6. Elemental profiles obtained at 4 kV (a) in the surface region of a SiO_x particle, (b) in the surface region of a graphite particle, and (c) in the interface region between a SiO_x and a graphite particle.

To complete these observations, a quantification (4 kV) of the elements Si, O, C, F, and P was carried out at different locations on the electrode sample cut with FIB (identified in Figure S9a), on the surface

of a SiO_x particle (Figure 6a), at the surface of a GHDR graphite particle (Figure 6b), and at the interface between SiO_x and graphite particles (Figure 6c). For the first two, the element detection intensity profiles are reported over a depth of about 1 µm, along a line starting from the porosity, crossing the SEI, and ending inside the particles, and are averaged over a width of about 1 µm. Although the interaction pear of the electron beam with the electrode material reaches a maximum of 0.2 µm at 4 kV (and 0.8 at 10 kV), these intensity profiles highlight the presence of an oxygen-rich SEI on the surface of the SiO_x particles (in the 0.2-0.6 µm length region of Figure 6a), also containing carbon, and to a lesser extent fluorine, and then phosphorus. The SEI appears thinner on the surface of the graphite (region 0.5-0.75 µm length of Figure 6b). These SEIs are also observed at the interface between a particle of SiO_x and graphite (regions 0.5-0.7 and 0.9-1.25 µm length of Figure 6c).

The morphology of the electrodes therefore changes significantly during cycling. There is a dilation of the electrode (thickness increase), which likely results in a mechanical loss of the electrical contacts between the SiO_x and graphite particles. There is a growth of an SEI, more particularly on the surface of the SiO_x particles, which likely increases the resistance to the lithium insertion and can also lead to a loss of electrical contacts. All these observations are consistent with the analysis of the incremental capacity curves which shows that the loss of capacity is mainly attributable to SiO_x. However, we do not notice a clear increase of the estimated polarization between cycle 5 to 60, especially for high coverage ratio (Figure S1a-b-c), whereas we would expect such a rise if the SEI growth was the SiO_x particles insulation source. We are therefore more convinced by the mechanical isolation of the SiO_x particles than a passivation by the SEI. The influence of the coverage ratio on the cyclability of the electrodes is probably attributable to the role of the binder in maintaining the mechanical contacts. As a matter of fact, Table 2 reports comparisons of the electrodes thickness (as measured with a micrometre) and porosity (calculated from the components mass fractions and densities) before and after cycling of several electrodes of the 10SFG-*xPAA* series. It can be seen that with the increase in the coverage ratio from 8 to 17 mg m^{-2}, the thickness and the porosity of the electrode increases less. Interestingly, the electrode dilation does not vary for an increase in the coverage ratio from 17 to 25 mg m^{-2}, which is in good agreement with the levelling of the capacity loss above the coverage ratio of 17 mg m^{-2}. It has also been reported that the binder can act as an artificial passivation layer, minimizing the direct contact between the surface of the active materials and the electrolyte, thus reducing the degradation of the latter. We did not conduct an analysis that would allow us to study the influence of the recovery rate on the quantity of SEI formed in the electrodes, which could have supported this hypothesis.

Table 2: Electrode thickness and porosity evolution between pristine state and after 60 cycles for different electrode composition from 10SFG-xPAA study.

	Coverage ratio Γ * (mg m^{-2})	Pristine state		60 cycles ageing		ΔThickness (%)
		Thickness (µm)	Porosity (%)	Thickness (µm)	Porosity (%)	
10SFG-2PAA-2SBR	8.3	74.8	34.5	110.0	57.1	47.2%
10SFG-7PAA-2SBR	17.2	79.7	36.5	99.7	50.4	25.1%
10SFG-11PAA-2SBR	24.9	86.0	36.3	110.7	51.6	28.7%

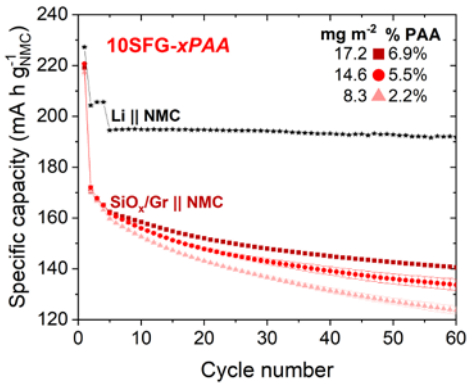

Figure 7. Cyclability of a SiO_x/Gr || NMC811 full cell, made with 10SFG-xPAA and half-cell Li || NMC811 with 1M $LiPF_6$ in FEC/DMC (3:7) electrolyte: capacity expressed in mA h per g of NMC811.

Electrochemical measurements – Full cells

Finally, we have assembled full cells with positive electrodes based on NMC 811 versus SiO_x/Gr electrodes (10SFG-*xPAA* series) to look at the influence of the coverage ratio in such configuration. So far, we put the problem of irreversible lithium consumption aside to focus on negative electrode mechanical limitations. Indeed, in half-cell configuration Li || SiO_x/Gr, the capacity of the metallic lithium electrode was at least 20 time greater than the SiO_x/Gr one. This huge excess of lithium, considered as infinite, compensates the irreversible consumption of lithium and electron (Li^+/e^-) caused by the initial silica reaction from SiO_2 to Li_4SiO_4[43,44,45,46] and the continuous creation of SEI caused by SiO_x swelling. On the opposite, in full cell configuration SiO_x/Gr || NMC, the capacity balance between the negative and the positive electrode is close to one meaning that the irreversible consumption of Li^+/e^- become a major issue. Therefore, we did a preliminary study in full cell configuration about the electrolyte effect on our SiO_x/Gr electrode cyclability. The first two

electrolytes correspond to the first generation of electrolytes envisioned for silicon-based electrodes, namely a conventional formulation (of the LP30 and LP40 type) based on ethylene carbonate (EC) with 10% additives of ethylene fluorocarbonate (FEC) or a mixture 10% FEC and 2% vinylidene carbonate (VC). The third electrolyte, which belongs to a second generation, does not contain EC, but a mixture of FEC and dimethyl carbonate (DMC)[10]. With such type of electrolyte, for example, Yang et al.[56], showed a significantly improved cyclability of SiO_x||$LiFePO_4$ cells compared with that of routine EC-based electrolyte. They have observed after cycling a better retention of the electrode microstructure and the formation of a low impedance LiF-rich SEI in this electrolyte compared to a high impedance Li_2CO_3-rich SEI in the routine electrolyte. The results obtained with a 10SFG-7PAA-2SBR electrode and the three electrolytes are represented in Figure S10a, establishing without question the superiority of the electrolyte without EC. Subsequently, only this EC-free electrolyte was kept, and full cells were assembled with 10SFG-*xPAA* series SiO_x/Gr electrodes from the optimum ratio to lower ratio.

Capacity results in Figure 7a are expressed in mA h per g of NMC (mA h g^{-1}_{NMC}). For each of the three coverage ratios they are about 219 ± 2 mA h g^{-1}_{NMC} and 171 ± 1 mA h g^{-1}_{NMC} for cycle 1 and 2 respectively. These capacities are clearly lower than the 227 ± 0.3 mA h g^{-1}_{NMC} and 204 ± 0.4 mA h g^{-1}_{NMC} of NMC half-cell reference versus metallic lithium. Such difference observed at cycle 1 could be explained by the N/P ratio lower than 1 (≈0.97) meaning that a part of lithium is still in the cathode after the first charge of the system. We assumed to overload the capacity of the positive electrode to offset the low initial efficiency of SiO_x material. Many studies aim to prelithiate the negative electrode by different technics but that is not our objective in this work. After the first discharge, the irreversible reactions of the cathode (ICE ≈ 89%) lead to an estimate N/P ratio of ≈1.1.

However, the gap of capacity of 32 mA h g^{-1}_{NMC} between half-cell and full cell at cycle 2 is the first sign of the irreversible consumption of Li^+/e^-. Although the NMC half-cells capacity decreases to 195 ± 0.2 mA h g^{-1}_{NMC} at the 5th cycle because of the C-rate increase (C/20 to C/5), this capacity remains stable and high equal to 192 ± 0.2 mA h g^{-1}_{NMC} after 60 cycles. On the opposite, capacities of SiO_x/Gr || NMC full cells decrease cycle after cycle to reach 124 ± 2 mA h g^{-1}_{NMC} for 10SFG-2PAA-2SBR electrode, 134 ± 2 mA h g^{-1}_{NMC} for 10SFG-5PAA-2SBR and 141 ± N/A mA h g^{-1}_{NMC} for 10SFG-7PAA-2SBR. The best performance is thus obtained at the optimal coverage ratio of ≈18 mg cm^{-2}. This result confirms that this parameter of the electrode formulation is a pertinent one.

Conclusion

The capacity fading upon cycling of SiO_x/Gr electrodes is the consequence of their expansion, following the volume variations of the SiO_x and the growth of the SEI on its surface. This results in a loss of the electrical connection of the SiO_x particles which then become inactive. The increase in the content of binder, which attaches the particles together, can counteract this expansion to a certain extent and minimize the degradation of the electrodes. For mixtures of SiO_x/Gr varying by the nature of the graphite, an optimal content of the binder, a mixture of PAA and SBR, has been identified and rationalized in terms of coverage ratio. The value of 18-20 mg of binder per m² of BET surface deployed by the SiO_x and carbon powders makes it possible to minimize fading, without affecting the kinetics (polarization) of the electrodes if the SBR content is kept below 8.7 mg_{SBR} m^{-2}. This binder, essential to ensure the necessary flexibility of the electrodes for their battery assembly, slows down the transport of ions within the electrode. The nature of the electrolyte influences the cycling of SiO_x/Gr electrodes. Interesting results were obtained in full cell vs. NMC 811 with an EC-free and FEC-rich electrolyte. The fading of the electrodes is minimized at the optimal coverage ratio. This coverage ratio therefore appears as an essential and convenient parameter of the formulation of electrodes to facilitate their optimization. Indeed, the optimal coverage ratio being known from a previous work, it can be then used to design *a priori* the formulation of an electrode made for a new electrode material, but keeping the same binder system. The only preliminary work required being the measurement (if unknown) of the specific surface area. This approach should therefore fasten the comparison of different grades (e.g. different granulometry) of a given active material, of different compositions of blends of active materials, or the optimization of conducting additive content. However, the optimal coverage ratio is likely to change depending on the binder characteristics, such as chemical formula and macromolecular architecture, and in the case of electrode material showing volume variations, with its content in the electrode as the mechanical stress sustained by the polymer bridges will depend on the extent of dilation/contraction of the electrode.

Experimental

Materials

All electrode components are industrial grades. The silicon-based material is a silicon oxide covered by graphene sheets (SiO_x, $x \approx 1$) from a graphene supplier ($D_{50} \approx 10$ µm, specific surface area ≈ 1.4 $m^2 g^{-1}$, specific capacity ≈ 1400 mA h g^{-1}). Graphite active materials used are GHDR 15-4 (D90 = 23 µm, specific surface area ≈ 4 $m^2 g^{-1}$ – Imerys) and SFG6L (D90 = 5.3 - 7.3 µm, specific surface area ≈ 17 $m^2 g^{-1}$ – Imerys) with a theoretical capacity of 372 mA h g^{-1}. C-NERGY™ SUPER C45 was used as conductive carbon additive (grit 20 µm = 12 ppm, specific surface area ≈ 45 $m^2 g^{-1}$ – Imerys). PolyAcrylic acid (PAA, Mw = 450 000 g mol^{-1} - Sigma-Aldrich) neutralized with a $LiOH.H_2O$ salt (Sigma-Aldrich, white crystal) was used as binder. In addition, the Styrene-Butadiene Rubber (SBR – BM-451B) from Zeon Corporation was used to complete PAA. NMC cathodes were prepared with NMC 811 (T81R – Shanshan) conductive carbon C-NERGY™ SUPER C65 (Imerys) and PVdF binder (Solef® 5130 - Solvay) in N-methyl-2-pyrrolidone (NMP – Alfa Aesar) as binder solution.

Electrodes preparation

Details of anodes composition are gathered in Table 1. Binder solutions for SiO_x/Graphite anode were prepared by mixing PAA and water with a magnetic stirrer. As shown in Table 1, the binder amount has been varied from a slurry to another. However, the higher the binder amount, the more viscous the slurry is. Therefore, in order to prepare slurries with similar viscosity, the binder concentration was adapted, varying between 2.4 and 7.4 wt%. Finally, the pH of PAA solutions was adjusted at 4.0 ± 0.1 with the $LiOH.H_2O$ salt, estimated at less than 0.1 wt% of the binder solution and of the final electrodes.

SiO_x/Graphite electrode slurries were prepared by mixing the binder solution with other electrode components thanks to a planetary blender (Thinky mixer ARE 250). This equipment does not contain grinding balls in contrary to a ball-miller, which may break silicon particles or binder chains[41] 41. SiO_x/Graphite balance is kept to 23:77 for all studied compositions. The powder of each electrode component was incorporated successively, and binder solution was then progressively added to form the electrode slurry (mix steps in Table S1). The slurry was coated onto an 8 µm copper foil and dried according to the following process: 10 min. at 30°C, a subsequent temperature ramp to reach 110°C in ≈ 35 min. and finally 30 min. at 110°C. This drying process has been selected to remain as close as possible to what is done in the industry where the drying step is done directly after the electrode coating and as fast as possible to increase production performance. The wet thickness was adapted for each slurry to obtain a surface capacity of 5.1 ± 0.3 mA h cm^{-2}, which is typical for an industrial negative electrode. A graphite anode is usually ≈ 14 mg_{AM} cm^{-2} to reach 5.1 mA h cm^{-2}, which is ≈ 67% heavier than the ≈ 8.4 mg_{AM} cm^{-2} needed for our SiO_x-based electrodes. After the drying step, electrodes were

then calendered at 1.5 t cm^{-2} with a rolling press (Medlab P – Ingecal) at 50°C to reach a porosity between 30 and 40% as requested in the industry[1] [1]. Porosity was calculated from the components mass fractions and densities thanks to a thickness measurement of each electrode by a micrometer (Mitutoyo).

NMC cathode slurries were prepared by mixing PVdF binder solution, carbon black and NMC active material during 90 min. in a stirring machine (ultra turrax® - IKA) following steps detailed in Table S2. Electrodes were coated onto a 15 µm aluminium foil and dried from 65°C to 130°C during 75 min. and then 60 min. at 130°C under vacuum. Electrodes were then calendered at 0.5 t cm^{-2} to reach a porosity between 30 and 40%.

Finally, 15 mm diameter circular electrodes were punched out and dried 3-4 hours at 100°C under vacuum in a Büchi before entering the glove box and coin cell assembling.

Electrochemical measurements – Half cells

SiO_x/Graphite electrodes were first tested in coin cell versus metallic lithium. They were assembled in glove box under argon atmosphere. A glass-fibre Whatman GF/D and a trilayer microporous membrane (PP/PE/PP) Celgard H2021 were used as separators. They were soaked with 200 µL electrolytic solution of 1 M $LiPF_6$ in ethylene carbonate (EC) and dimethyl carbonate (DMC) 1:1 + 10 wt% fluoroethylene carbonate (FEC). SiO_x/Graphite electrodes were employed as the working electrodes with lithium foil as both counter and reference electrodes. The cycling tests were performed in galvanostatic mode at 23°C within the potential window of 1 – 0.01 V versus Li^+/Li. The theoretical C-rate based on the theoretical capacity of 607 mA h g^{-1} (according to SiO_x/Graphite weight ratio of 23:77) was fixed at C/20 for the first three cycles (full capacity in 20h). The third cycle was then used to define the experimental capacity of the SiO_x/Graphite electrode in order to apply a real C/5 rate for the next 57 cycles. For all cycles, a constant current (CC) followed by a constant voltage (CV) step at the end of the SiO_x/Graphite electrode lithiation are applied. This floating step at 10 mV was maintained until the measured current reached an equivalent of a C/50 value or a duration of more than two hours. For the sake of reproducibility, two to three cells were tested for each SiO_x/Graphite electrode formulation, and the results were averaged.

Electrochemical measurements – Full cells

Some SiO_x/Graphite electrodes were tested in coin cell versus NMC cathode. The electrolytic solution could be 1 M $LiPF_6$ in EC:DMC 1:1 + 10 wt% FEC or 1 M $LiPF_6$ in EC:EMC 3:7 + 2 wt% VC + 10 wt% FEC or 1 M $LiPF_6$ in FEC:DMC 3:7. The same cycling sequence was used within a 2.5 – 4.2 V potential window. A CV step at 4.2 V was also used to reach complete lithiation of the SiO_x/Graphite anode until the measured current reached an equivalent of a C/50 value or a duration of more than two hours.

Usually, the capacities ratio between the negative and positive electrode (N/P) is close to 1.1. However, this ratio is common for Graphite/NMC battery in which each active material exhibits usually a low initial irreversible capacity. On the opposite, the typical irreversible capacity of SiO_x for the first electrochemical cycle corresponds to approx. 50%[43] [43] of the first discharge capacity against 15% for the graphite. This is not a problem in half cell versus metallic lithium because the lithium/electron source is regarded as infinite. The cyclability is not impacted by the lithium consumption corresponding to the irreversible capacity contrary to the full cell case where lithium ion source is finite (here in the NMC electrode). To overcome such limitation a pre lithiation of the SiO_x material can be done and would be applicable for an industrial approach[46] [46]. Nevertheless, in our case, we decided to increase the mass loading, and thus the capacity, of the NMC cathode to take into account the lithium lost in the initial SEI formation during the first lithiation of the SiO_x/Graphite anode. In the present study, we targeted a N/P ratio ≈ 1,1 on the second cycle when the main part of the irreversible capacities is over. This choice lead to a N/P ratio lower than 1 (≈ 0,96) which is uncommon in the industry because of the lithium dendrite growing risk. NMC cathode mass loading was 28-31 mg_{AM} cm^{-2}.

Mechanical measurements - The peel strength

The electrode samples were cropped to strips of 15 × 100 mm^2. For 180° peeling tests set-up, a double-sided adhesive 3M-468MP tape was stuck on a metal vertical plate where the electrode coating was pasted on. On the other electrode side, current collector was attached to another similar tape. The peeling force was carried out with 180° peeling tests (Zwick Roell Z010) by pulling that later tape at a speed of 100 mm min^{-1} during 80 mm length. We peeled 2 or 3 samples per composition and averaged adhesive force.

Mechanical measurements - Winding test

Pieces of electrode were rolled and taped around a metal bar with a diameter of three millimetres in order to simulate the radius of curvature of a cylindrical type lithium-ion battery. Bars were directly observed by SEM to see damages caused by the winding. Some post-processing was done to evaluate crack widths and crack surface density. We used the local thickness method of Fiji software (ImageJ) which evaluate for each point of the crack the largest sphere diameter that fits inside the crack and contains the point[48] [48].

Electrical measurements – 4 probes test

The electronic resistivity of the SiO_x/Graphite electrodes was measured by using four-point probe mapping system (model 280SI-Microword) with computer controlled stepping motors to move the four-point probe. The spacing between each probe is 1 mm. Each probe has a contact area radius of

100 mm and the load applied on each probe is 60 g. ≈ 3×3 - 4×4 cm² electrode sqares were measured at 30-50 spots.

Scanning electron microscopy (SEM) & Cross section achievement

To observe the morphology of the electrodes before and after cycling, they were rinsed by immersion in DMC then included in a polymerizable resin (Struers CaldoFix-2 polymerized two days at ambient temperature). Cuts were then made using a cross section polisher (JEOL SM-09010). This method makes it possible to minimize the exposure and evolution of the samples to air. Then a scanning electron microscope (SEM – JEOL JSM 7600F, Hitachi TM3000, FIB/SEM ZEISS Cross Beam 550 FIB) was used to visualize the electrode morphology. For the X-ray spectroscopy (EDX) analysis, we used Aztec Advanced Software and Oxford SDD detector. First, a cross section of a cycled electrode without resin was generated by using the FIB/SEM to create the sample and then scanning by EDX. We obtained elemental mappings of Si, C, O, F and P, an electron energy of 4 and 10 kV was selected.

Analysis of incremental capacity curves

Derivative of the capacity with respect to the voltage data were calculated using the EC-Lab® software (BioLogic). A post-processing of these data was done with a home-made routine written using Python™. The aim of the routine was to treat a significant data quantity to discriminate the capacity contributions of each active material.

Acknowledgements

Nicolas Stephant, Cassandre Chalard, and Nicolas Goubard are thanked for fruitful discussions.

References

[1] M. Armand, P. Axmann, D. Bresser, M. Copley, K. Edström, C. Ekberg, D. Guyomard, B. Lestriez, P. Novak, M. Petranikova, W. Porcher, S. Trabesinger, M. Wohlfahrt-Mehrens, H. Zhang, "Lithium-ion batteries – Current state of the art and anticipated developments", J. Power Sources, 479, 2020, 228708

[2] T. Chen, J. Wu, Q. Zhang, X. Su, "Recent advancement of SiO_x based anodes for lithium-ion batteries", J. Power Sources, 363 (2017) 126-144

[3] X. Zhu, B. Liu, J. Shao, Q. Zhang, Y. Wan, C. Zhong, J. Lu, Fundamental Mechanisms and Promising Strategies for the Industrial Application of SiO_x Anode, Adv. Funct. Mater. 2023, 2213363

[4] D. Mazouzi, Z. Karkar, C. Reale Hernandez, P. Jimenez Manero, D. Guyomard, L. Roué, B. Lestriez, "critical roles of binders and formulation at multiscales of silicon-based composite electrodes", J. Power Sources, 2015, 280, 533-549

[5] A. Magasinski, B. Zdyrko, I. Kovalenko, B. Hertzberg, R. Burtovyy, C.F. Huebner, T.F. Fuller, I. Luzinov, G. Yushin, "Toward Efficient Binders for Li-Ion Battery Si-Based Anodes: Polyacrylic Acid", J. Appl. Mater. Interfaces 2 (2010) 3004.

[6] Z. Karkar, D. Guyomard, B. Lestriez, L. Roué, "A comparative study of polyacrylic acid (PAA) and carboxymethyl cellulose (CMC) binders for Si-based electrodes", Electrochimica Acta, 2017, 258, 453-466

[7] L. Huet, P. Moreau, N. Dupré, T. Devic, L. Roué, B. Lestriez, "Nanoscale Morphological Characterization of Coordinated Binder and Solid Electrolyte Interphase in Silicon-Based Electrodes for Li-ion Batteries", Small Methods, 2022, 2200827

[8] S. Aoki, Z.-J. Han, K. Yamagiwa, N. Yabuuchi, M. Murase, K. Okamoto, T. Kiyosu, M. Satoh and S. Komaba, "Acrylic Acid-Based Copolymers as Functional Binder for Silicon/Graphite Composite Electrode in Lithium-Ion Batteries", J. Electrochem. Soc., 2015, 162, A2245–A2249

[9] F. Jeschull, F. Lindgren, M. J. Lacey, F. Björefors, K. Edström, D. Brandell, "Influence of inactive electrode components on degradation phenomena in nano-Si electrodes for Li-ion batteries", J. Power Sources 325 (2016) 513-524

[10] J. Xiong, N. Dupré, P. Moreau, B. Lestriez, "From the direct observation of a PAA based binder using STEM-VEELS to the ageing mechanism of silicon/graphite anode with high areal capacity cycled in an FEC-rich and EC-free electrolyte", Adv. Energy Mater., 2022, 2103348

[11] N. Yabuuchi, K. Shimomura, Y. Shimbe, T. Ozeki, J.-Y. Son, H. Oji, Y. Katayama, T. Miura, S. Komaba, "Graphite-Silicon-Polyacrylate Negative Electrodes in Ionic Liquid Electrolyte for Safer Rechargeable Li-Ion Batteries", Adv. Energy Mater., 1 (2011) 759.

[12] H. Woo, B. Gil, J. Kim, K. Park, A. J. Yun, J. Kim, S. Nam, B. Park, "Metal-Coordination Mediated Polyacrylate for High Performance Silicon Microparticle Anode", Batteries & Supercaps 2020, 3, 1287–1295

[13] L. Huet, D. Mazouzi, P. Moreau, N. Dupré, M. Paris, S. Mittelette, D. Laurencin, T. Devic, L. Roué, B. Lestriez, "Coordinatively Cross-linked Binders for Silicon-Based Electrodes for Li-ion Batteries: Beneficial Impact on Mechanical Properties and Electrochemical Performance", ACS Applied Materials & Interfaces, 15 (2023) 15509−15524

[14] Z. Xu, J. Yang, T. Zhang, Y. Nuli, J. Wang, S-i. Hirano, Silicon Microparticle Anodes with Self-Healing Multiple Network Binder, Joule 2, 950–961, 2018

[15] D-Y. Han, I. K. Han, H. B. Son, Y. S. Kim, J. Ryu, S. Park, Layering Charged Polymers Enable Highly Integrated High-Capacity Battery Anodes, Adv. Funct. Mater. 2023, 2213458

[16] P. Heugel, W. Märkle, T. Deich, O. von Kessel, J. Tübke, Thickness change and jelly roll deformation and its impact on the aging and lifetime of commercial 18650 cylindrical Li-ion cells with silicon containing anodes and nickel-rich cathodes, J. Energy Storage, 53 (2022) 105101

[17] A. Pfrang, A. Kersys, A. Kriston, R-G. Scurtu, M. Marinaro, M. Wohlfahrt-Mehrens, "Deformation from Formation until End of Life: Micro X-Ray Computed Tomography of Silicon Alloy Containing 18650 Li-Ion Cells", J. Electrochem. Soc., 2023, DOI 10.1149/1945-7111/acc6f3

[18] I. Profatilova, E. De Vito, S. Genies, C. Vincens, E. Gutel, O. Fanget, A. Martin, M. Chandesris, M. Tulodziecki, W. Porcher, “Impact of Silicon/Graphite Composite Electrode Porosity on the Cycle Life of 18650 Lithium-Ion Cell.” ACS Appl. Energy Mater., 3 (2020) 11873−11885.

[19] F. Jeschull, D. Brandell, M. Wohlfahrt-Mehrens, M. Memm, “Water-Soluble Binders for Lithium-Ion Battery Graphite Electrodes: Slurry Rheology, Coating Adhesion, and Electrochemical Performance”, Energy Technol., 5 (2017) 2108 – 2118

[20] S. Komaba, K. Shimomura, N. Yabuuchi, T. Ozeki, H. Yui and K. Konno, J. Phys. Chem. C, 2011, 115, 13487–13495

[21] C. Reale Hernandez, A. Etiemble, D. Mazouzi, Z. Karkar, E. Maire, D. Guyomard, B. Lestriez, L. Roué, “A Facile and Very Effective Method to Enhance the Mechanical Strength and the Cyclability of Si-Based Electrodes for Li-Ion Batteries”, Adv. Energy Mater, 2018, 8, 1701787

[22] V. Vanpeene, J. Villanova, A. King, B. Lestriez, E. Maire, L. Roué, “Dynamics of the morphological degradation of Si-based anodes for Li-ion batteries characterized by in-situ synchrotron X-ray tomography”, Adv. Energy Mater. 9, 2019, 1803947

[23] M. J. Jolley, T. S. Pathan, A. M. Wemyss, I. Prokes, S. Moharana, C. Wan, M. J. Loveridge, Development and Application of a Poly(acrylic acid)-Grafted Styrene−Butadiene Rubber as a Binder System for Silicon-Graphite Anodes in Li-Ion Batteries, ACS Appl. Energy Mater. 2023, 6, 496−507

[24] B. Lestriez, “Functions of polymers in composite electrodes of lithium ion batteries”, C. R. Chimie, 2010, 137, A1341-A1350

[25] K. Ambrock, M. Ruttert, A. Vinograd, B. Billmann, X. Yang, T. Placke, M. Winter, M. Börner, Optimization of graphite/silicon-based composite electrodes for lithium ion batteries regarding the interdependencies of active and inactive materials, Journal of Power Sources 552 (2022) 232252

[26] J. Xiong, N. Dupré, D. Mazouzi, D. Guyomard, L. Roué, B. Lestriez, "Influence of the polyacrylic acid binder neutralization degree on the initial electrochemical behavior of a silicon / graphite electrode”, ACS Applied Materials & Interfaces, 13, 2021, 28304−28323

[27] Y. Surace, F. Jeschull, P. Novák, S. Trabesinger, “Performance-Determining Factors for Si–Graphite Electrode Evaluation: The Role of Mass Loading and Amount of Electrolyte Additive”, J. Electrochem. Soc. 170 (2023) 020510

[28] J. Duchet, J.P. Chapel, B. Chabert, J.F. Gérard, “Effect of the Length of Tethered Chains and the Interphase Structure on Adhesion between Glass and Polyethylene”, Macromolecules, 31 (1998) 8264.

[29] C. Creton, E.J. Kramer, H.R. Brown, C.Y. Hui, “Adhesion and fracture of interfaces between immiscible polymers: from the molecular to the continuum scale”, Adv. Polym. Sci., 156 (2002) 53.

[30] S. Müller, P. Pietsch, B-E. Brandt, P. Baade, V. De Andrade, F. De Carlo, V. Wood, “Quantification and modeling of mechanical degradation in lithium-ion batteries based on nanoscale imaging”, Nat. Commun. 9 (2018) 2340

[31] U. Maver, A. Znidarsic, M. Gaberscek, J. Mater. Chem. 21 (2011) 4071

[32] A. Tranchot, H. Idrissi, P. X. Thivel, and L. Roué, Impact of the Slurry pH on the Expansion/Contraction Behavior of Silicon/Carbon/Carboxymethylcellulose Electrodes for Li-Ion Batteries, J. Electrochem. Soc. 163 (6) A1020-A1026 (2016)

[33] A. Li, J. Hempel, M. Balogh, Y-T. Cheng, A. Taub, “Effect of Binder Content on Silicon Microparticle Anodes for Lithium-Ion Batteries”, J. Electrochem. Soc., 170 (2023) 010533

[34] A. Tranchot, H. Idrissi, P.-X. Thivel, L. Roué, “Influence of the Si particle size on the mechanical stability of Si-based electrodes evaluated by in-operando dilatometry and acoustic emission”, J. Power Sources, 330 (2016) 253-260.

[35] B. Hu, I. A. Shkrob, S. Zhang, L. Zhang, J. Zhang, Y. Li, C. Liao, Z. Zhang, W. Lu, L. Zhang, “The existence of optimal molecular weight for poly(acrylic acid) binders in silicon/graphite composite anode for lithium-ion batteries”, J. Power Sources 378 (2018) 671–676

[36] N. Delpuech, D. Mazouzi, N. Dupre, P. Moreau, M. Cerbelaud, J-S. Bridel, J-C. Badot, E. De Vito, D. Guyomard, B. Lestriez, B. Humbert. “Critical Role of Si Nanoparticles Surface on Lithium Cell Electrochemical Performance Analyzed by FTIR, Raman, EELS, XPS, NMR and BDS Spectroscopies”, J. Phys. Chem. C, 118 (2014) 17318-17331

[37] P. Mandal, K. Stokes, G. Hernández, D. Brandell, J. Mindemark, “Influence of Binder Crystallinity on the Performance of Si Electrodes with Poly(vinyl alcohol) Binders”, ACS Appl. Energy Mater. 2021, 4, 3008−3016

[38] M. K. Burdette-Trofimov, B. L. Armstrong, L. Heroux, M. Doucet, A. E. Márquez Rossy, D. T. Hoelzer, N. Kanbargi, A. K. Naskar, G. M. Veith, “Competitive adsorption within electrode slurries and impact on cell fabrication and performance”, J. Power Sources 520 (2022) 230914.

[39] C.-C. Li, J.-T. Lee, X.-W. Peng, “Binder Distributions inWater-Based and Organic-Based $LiCoO_2$ Electrode Sheets and Their Effects on Cell Performance”, J. Electrochem. Soc., 153 (2006) A809.

[40] S. Jaiser, M. Müller, M. Baunach, W. Bauer, P. Scharfer, W. Schabel, "Microstructure formation of lithium-ion battery electrodes during drying - An ex-situ study using cryogenic broad ion beam slope-cutting and scanning electron microscopy (Cryo-BIB-SEM)", J. Power Sources, 318 (2016) 210.
[41] T. Chartrel, M. Ndour, V. Bonnet, S. Cavalaglio, L. Aymard, F. Dolhem, L. Monconduit, J.-P., Bonnet, "Revisiting and Improving the Preparation of Silicon-Based Electrodes for Lithium-Ion Batteries: Ball Milling Impact on Poly(Acrylic Acid) Polymer Binders", Mater. Chem. Front., 3 (2019) 881–891.
[42] Novák, P., Joho, F., Lanz, M., Rykart, B., Panitz, J. C., Alliata, D., ... & Haas, O. (2001). The complex electrochemistry of graphite electrodes in lithium-ion batteries. Journal of power sources, 97, 39-46.
[43] Y. Reynier, C. Vincens, C. Leys, B. Amestoy, E. Mayousse, B. Chavillon, L. Blanc, E. Gutel, W. Porcher, T. Hirose, C. Matsui "Practical implementation of Li doped SiO in high energy density 21700 cell", J. Power Sources, 2020, 450, 227699.
[44] Kitada, K., Pecher, O., Magusin, P. C., Groh, M. F., Weatherup, R. S., & Grey, C. P. (2019). Unraveling the reaction mechanisms of SiO anodes for Li-ion batteries by combining in situ 7Li and ex situ 7Li/29Si solid-state NMR spectroscopy. Journal of the American Chemical Society, 141(17), 7014-7027.
[45] Hirose, T., Morishita, M., Yoshitake, H., & Sakai, T. (2017). Investigation of carbon-coated SiO phase changes during charge/discharge by X-ray absorption fine structure. Solid State Ionics, 304, 1-6.
[46] Xin Li, Xiaohong Sun, Xudong Hu, Fengru Fan, Shu Cai, Chunming Zheng, Galen D. Stucky "Review on comprehending and enhancing the initial Coulombic efficiency of anode materials in lithium-ion/sodium-ion batteries", Nano Energy, 2020, 77, 105143.
[47] Li, J., Downie, L. E., Ma, L., Qiu, W., & Dahn, J. R. (2015). Study of the failure mechanisms of LiNi0. 8Mn0. 1Co0. 1O2 cathode material for lithium ion batteries. Journal of The Electrochemical Society, 162(7), A1401.
[48] Hildebrand, T., & Rüegsegger, P. (1997). A new method for the model-independent assessment of thickness in three-dimensional images. Journal of microscopy, 185(1), 67-75.
[49] Lee, J. H., Kim, J., Jeong, M. H., Ahn, K. H., Lee, H. L., & Youn, H. J. (2023). Visualization of styrene-butadiene rubber (SBR) latex and large-scale analysis of the microstructure of lithium-ion battery (LIB) anodes. Journal of Power Sources, 557, 232552.
[50] Kaneko, M., Nakayama, M., & Wakihara, M. (2007). Lithium-ion conduction in elastomeric binder in Li-ion batteries. Journal of Solid State Electrochemistry, 11, 1071-1076.
[51] Guy, D., Lestriez, B., Bouchet, R., & Guyomard, D. (2006). Critical role of polymeric binders on the electronic transport properties of composites electrode. Journal of The Electrochemical Society, 153(4), A679.
[52] Seïd, K. A., Badot, J. C., Dubrunfaut, O., Levasseur, S., Guyomard, D., & Lestriez, B. (2012). Influence of the carboxymethyl cellulose binder on the multiscale electronic transport in carbon–$LiFePO_4$ nanocomposites. Journal of Materials Chemistry, 22(45), 24057-24066.
[53] Yao, K. P., Okasinski, J. S., Kalaga, K., Almer, J. D., & Abraham, D. P. (2019). Operando quantification of (de) lithiation behavior of silicon–graphite blended electrodes for lithium-ion batteries. Advanced Energy Materials, 9(8), 1803380.
[54] Dupré, N., Moreau, P., De Vito, E., Quazuguel, L., Boniface, M., Bordes, A., ... & Guyomard, D. (2016). Multiprobe study of the solid electrolyte interphase on silicon-based electrodes in full-cell configuration. Chemistry of Materials, 28(8), 2557-2572.
[55] Eshetu, G. G., & Figgemeier, E. (2019). Confronting the challenges of next-generation silicon anode-based lithium-ion batteries: role of designer electrolyte additives and polymeric binders. ChemSusChem, 12(12), 2515-2539.
[56] Yang, Y., Li, Z., Xu, Y., Yang, Z., Zhang, Y., Wang, J., ... & Zhao, H. (2023). Boosting fast electrode reaction kinetics of silicon suboxide anodes by fluoroethylene carbonate-based electrolyte. Journal of Power Sources, 577, 233261.